BIOCHEMISTRY
including biophysical chemistry & molecular biology

Article

pubs.acs.org/biochemistry

Interaction between the D2 Dopamine Receptor and Neuronal Calcium Sensor-1 Analyzed by Fluorescence Anisotropy

Matthew P. Woll,[†] Dan A. De Cotiis,[‡] Maria C. Bewley,[‡] Diana M. Tacelosky,[†] Robert Levenson,[†] and John M. Flanagan*[,‡]

[†]Department of Pharmacology and [‡]Department of Biochemistry and Molecular Biology, Pennsylvania State University College of Medicine, Hershey, Pennsylvania 17033, United States

Supporting Information

ABSTRACT: Neuronal calcium sensor-1 (NCS-1) is a small calcium binding protein that plays a key role in the internalization and desensitization of activated D2 dopamine receptors (D2Rs). Here, we have used fluorescence anisotropy (FA) and a panel of NCS-1 EF-hand variants to interrogate the interaction between the D2R and NCS-1. Our data are consistent with the following conclusions. (1) FA titration experiments indicate that at low D2R peptide concentrations calcium-loaded NCS-1 binds to the D2R peptide in a monomeric form. At high D2R peptide concentrations, the FA titration data are best fit by a model in which the D2R peptide binds two NCS-1 monomers sequentially in a cooperative fashion. (2) Competition FA experiments in which unlabeled D2R peptide was used to compete with labeled peptide for binding to NCS-1 shifted titration curves to higher NCS-1 concentrations, suggesting that the binding of NCS-1 to the D2R is highly specific and that binding occurs in a cooperative fashion. (3) N-Terminally myristoylated NCS-1 dimerizes in a calcium-dependent manner. (4) Co-immunoprecipitation experiments in HEK-293 confirm that NCS-1 can oligomerize in cell lysates and that oligomerization is dependent on calcium binding and requires functionally intact EF-hand domains. (5) Ca^{2+}/Mg^{2+} FA titration experiments revealed that NCS-1 EF-hands 2−4 (EF2−4) contributed to binding with the D2R peptide. EF2 appears to have the highest affinity for Ca^{2+}, and occupancy of this site is sufficient to promote high-affinity binding of the NCS-1 monomer to the D2R peptide. Magnesium ions may serve as a physiological cofactor with calcium for NCS-1−D2R binding. Finally, we propose a structural model that predicts that the D2R peptide binds to the first 60 residues of NCS-1. Together, our results support the possibility of using FA to screen for small molecule drugs that can specifically block the interaction between the D2R and NCS-1.

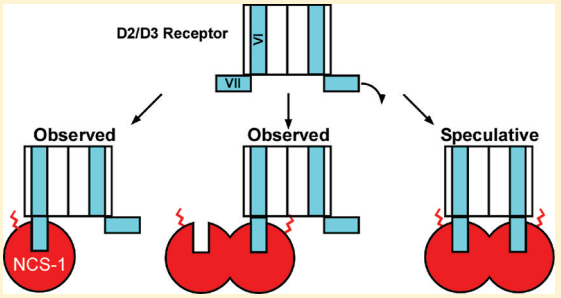

Neuronal calcium sensor-1 (NCS-1) is the primordial member of the neuronal calcium sensor (NCS) family of EF-hand calcium binding proteins that includes recoverin, neurocalcin, hippocalcin, VILIP-1−3, guanylate cyclase-activating proteins (GCAPs), and Kv channel-interacting proteins (KChIPs).[1] NCS-1 is the mammalian ortholog of frequenin, a protein critical for synaptic transmission within the *Drosophila* nervous system.[2] In mammalian cells, NCS-1 has been shown to promote exocytosis from dense core vesicles in both neurons and neuroendocrine cells[3] and plays a key role in G-protein-coupled receptor desensitization via a direct interaction with the D2 dopamine receptor (D2R).[4] Characterization of the R102Q NCS-1 variant, identified in an individual with autism, resulted in the rapid cycling between cytosolic and membrane pools in mouse N2A neuroblastoma cells.[5] Further, an increased level of expression of NCS-1 has been observed in the prefrontal cortex of individuals with schizophrenia and bipolar disorder[6,7] and is upregulated in injured neurons and in epilepsy,[8,9] suggesting that the D2R−NCS-1 interaction may represent a novel target for the development of drugs that may be useful for the treatment of these increasingly prevalent diseases.

NCS-1, in common with all NCS family members, contains four EF-hand domains. The EF-hand motif is a 12-residue loop flanked on either side with an α-helix.[10] In NCS family members, typically three of these motifs bind calcium with low to midnanomolar affinity and Hill coefficients of ∼2 (for a review, see ref 11). Most members contain N-terminal myristoylation consensus sequences (excluding KChIP2 and KChIP3)[11] that may be involved in membrane targeting. In NCS-1 specifically, the first EF-hand (EF1) does not bind Ca^{2+} because of the substitution of cysteine and proline residues at critical positions in the first helix (for a review, see ref 11). Calcium is a known regulator of NCS-1 function. In vivo experiments have demonstrated that Ca^{2+} binding modulates the functional interaction of NCS-1 with the D2R and other binding partners to affect cellular signaling.[4,12−14] However, the detailed mechanism(s) by which calcium modulates these effects is unclear.

Received: April 26, 2011
Revised: August 6, 2011
Published: August 29, 2011

Calcium ion binding has been previously shown to promote a set of conformational changes in NCS-1 that stabilize the native, functional conformation required for binding to its cellular partners.[15] In general, the oligomeric state of NCS-1 in its signaling complex(es) is unknown; however, several other NCS family members self-associate in response to changes in calcium ion concentrations[16,17] or form covalent disulfide linkages when saturated with Ca^{2+}.[18] The formation of NCS-1 oligomers could provide multiple binding regions for interaction with several different binding partners or alternatively form a single binding domain contributed by multiple monomer subunits.

In this study, we have used fluorescence anisotropy (FA) and a panel of NCS-1 variants to assess the contribution of Ca^{2+} binding to the interaction between the D2R and NCS-1. Our experiments support the idea that the D2R and NCS-1 form a high-affinity calcium-dependent complex that requires occupancy of all three calcium-binding EF-hands for optimal stability. The results presented here provide new insight into the regulation and assembly of the D2R·NCS-1 complex and highlight the possibility of using FA as a tool to screen for compounds capable of specifically blocking the association between the D2R and NCS-1.

EXPERIMENTAL PROCEDURES

NCS-1 Expression and Purification. All NCS-1 constructs either contained a C-terminal His_6 tag[19] or were engineered with a TEV protease cleavable N-terminal His_6 tag within the pET-28-TEV vector (gift of S. Burley, SGX Pharmaceuticals, San Diego, CA). Site specific variants E84Q (within EF2), E120Q (within EF3), and E168Q (within EF4) and the NCS-1ΔEF (E84Q/E120Q/E168Q) variant (within EF2−4) were generated using a Quikchange site-directed mutagenesis kit (Stratagene). All mutations were verified by direct DNA sequencing.

Each recombinant NCS-1 protein was overexpressed in *Escherichia coli* BL21(DE3) cells (Novagen) grown in ZYP-5052 autoinduction medium[20] and purified by nickel-nitriloacetic acid (NiNTA) affinity chromatography as previously described.[19] The cleavable N-terminal His_6 tag on the pET-28-TEV-expressed NCS-1 fusion protein was removed by an overnight digestion with His_6-tagged TEV protease (50:1 NCS-1:TEV) followed by an additional round of NiNTA affinity chromatography. The resulting protein (NCS-1 TEV) contains a residual glycine-histidine-methionine vector sequence present at the N-terminus of the endogenous NCS-1 sequence. All of the bacterially expressed proteins were further purified by gel filtration chromatography on a Superdex 75 10/300 GL gel filtration column (GE Healthcare Lifesciences) equilibrated in sample buffer [1 mM dithiothreitol (DTT), 20 mM HEPES, and 100 mM NaCl (pH 7.5)] where they eluted as monomers, as judged by multiangle light scattering and refractive index detection (Wyatt Technology Corp., Santa Barbara, CA).

Fractions containing purified NCS-1 proteins were incubated overnight in gel filtration buffer containing 50 mM EGTA to remove free and protein-bound calcium and magnesium. Calcium was subsequently removed, to a subnanomolar concentration, by buffer exchange against Chelex 100 (Bio-Rad)-treated buffer containing 20 mM HEPES and 100 mM NaCl (pH 7.5) using an Amicon Ultra centrifugal concentrator. The residual calcium and magnesium concentrations of the final purified NCS-1 protein were determined by atomic absorption (Huffman Laboratories Inc.) to be ∼47 and ∼3 nM, respectively, corresponding to ion:NCS-1 ratios of 1:100 and 1:1700, respectively.

Synthesis and Labeling of the D2R Peptide Tracer. A 17-amino acid residue peptide corresponding to the C-terminal tail of the D2R (residues 428−443, spanning the NCS-1 binding site) with an additional lysine residue was synthesized (New England Peptide) and used for binding experiments. For fluorescence experiments, a fluorescein-labeled peptide (D2R-FL) (TFNIEFRKAFLKILHCK-fluorescein) was synthesized to include a C-terminal lysine that provided a site for fluorophore attachment. MALDI-TOF MS analysis indicated a purity of >95% for the D2R-FL peptide. An unlabeled D2R peptide (uD2R) containing an acetylated C-terminus instead of fluorescein was also synthesized (Proteomics Core Facility, Pennsylvania State University College of Medicine). The unlabeled peptide was purified by reverse phase high-performance liquid chromatography (HPLC) and analyzed by MALDI-TOF MS. Labeled and unlabeled peptides were lyophilized and resuspended in water containing 1 mM DTT and 0.001% Tween 20 (pH 7.5). The concentration of the D2R-FL peptide was determined from its absorbance at 490 nm (Molecular Probes Handbook), and the concentration of the unlabeled D2R peptide was determined as previously described.[21]

Fluorescence Anisotropy. Fluorescence anisotropy (FA) was assessed using an ISS PC1 fluorimeter (ISS Corp.) equipped with Glan-Thompson polarizers on emission and excitation channels. All measurements were taken at 30 °C (Peltier-controlled) in a 10 mm special optical glass cuvette (Starna Cells, catalog no. 3/SOG/10) with a reaction volume of 1.5 mL of a buffer containing 20 mM HEPES, 100 mM NaCl, and 2 mM DTT (pH 7.5). Samples were excited at 490 nm, and the emission was monitored at 530 nm with a cutoff filter (Schott OG-515) and a band-pass filter (Ealing catalog no. 35-3607) having a 10 nm bandwidth.

FA titration experiments were performed by serial dilution of saturating concentrations of NCS-1 in buffer containing 1 nM D2R-FL, 20 mM HEPES, 100 mM NaCl, 2 mM DTT, and 2 mM $CaCl_2$ (pH 7.5) with the same solution lacking NCS-1. This method results in NCS-1 concentrations that are equally spaced on a logarithmic scale. Because of differences in the affinity of NCS-1 variants for the D2R-FL peptide, the final protein concentration was adjusted for each NCS-1 variant tested (as indicated in the figure legends). For competition FA titrations, samples contained 1 nM D2R-FL and 0, 1, or 5 μM uD2R, at a saturating concentration of NCS-1 TEV (5 μM).

For calcium FA titrations, serial additions of $CaCl_2$ were made to samples containing 1 nM D2R-FL and either 1, 5, or 10 μM NCS-1 TEV. For calcium/magnesium FA titrations, serial additions of $CaCl_2$ were made to samples containing 1 nM D2R-FL, 5 μM NCS-1, and either 0, 1, or 50 mM $MgCl_2$.

Data Analysis. The titration data for the binding of the D2R-FL peptide to NCS-1 TEV were fit to five models, in which the change in D2R-FL anisotropy reflects

Binding of a single NCS-1 monomer (model 1) to form D2R·NCS-1 complex:

$$A_{calc} = \frac{A_f + A_m K_{A1}[\text{NCS-1}]}{1 + K_{A1}[\text{NCS-1}]} \quad (1)$$

where A_{calc} is the expected anisotropy for the model, A_f and A_m are the anisotropies of free D2R-FL and D2R-FL bound to a single NCS-1 monomer, respectively, [NCS-1] is the total concentration of NCS-1 in the reaction mixture, and K_{A1}

(μM^{-1}) is the equilibrium association constant for complex formation.

Cooperative binding of two NCS-1 monomers (model 2) to form the D2R·$(NCS\text{-}1)_2$ complex:

$$A_{calc} = \frac{A_f + A_d K_{dimer}[NCS\text{-}1]^2}{1 + K_{dimer}[NCS\text{-}1]^2} \quad (2)$$

where K_{dimer} (μM^{-2}) is the equilibrium association constant for cooperative assembly of the 1:2 D2R-FL·$(NCS\text{-}1)_2$ complex from the free peptide and two NCS-1 monomers and A_d is the anisotropy of this complex. To facilitate comparison, the apparent equilibrium association constant, defined as $(K_{dimer})^{1/2}$ (μM^{-1}), was used. This value corresponds to the concentration of NCS-1 monomer that results in half-saturation of the 1:2 complexes.

Cooperative binding of three NCS-1 monomers (model 3) to form the D2R·$(NCS\text{-}1)_3$ complex:

$$A_{calc} = \frac{A_f + A_{tri} K_{trimer}[NCS\text{-}1]^3}{1 + K_{trimer}[NCS\text{-}1]^3} \quad (3)$$

where K_{trimer} (μM^{-3}; $K_{app,trimer} = K_{trimer}^{1/3}$) is the equilibrium association constant for the cooperative binding of three NCS-1 monomers and A_{tri} is the anisotropy of the 1:3 D2R-FL·$(NCS\text{-}1)_3$ species.

Sequential binding of two NCS monomers (model 4) to form D2R·NCS-1 and D2R·$(NCS\text{-}1)_2$ complexes:

$$A_{calc} = (A_f + A_m K_{A1}[NCS\text{-}1] + A_d K_{A1} K_{A2} [NCS\text{-}1]^2)/(1 + K_{A1}[NCS\text{-}1] + K_{A1} K_{A2}[NCS\text{-}1]^2) \quad (4)$$

Sequential binding of three NCS-1 monomers (model 5) to form D2R·NCS-1, D2R·$(NCS\text{-}1)_2$, and D2R·$(NCS\text{-}1)_3$ complexes:

$$A_{calc} = (A_f + A_m K_{A1}[NCS\text{-}1] + A_d K_{A1} K_{A2} [NCS\text{-}1]^2 + A_{tri} K_{A1} K_{A2} K_{A3} [NCS\text{-}1]^3) / (1 + K_{A1}[NCS\text{-}1] + K_{A1} K_{A2}[NCS\text{-}1]^2 + K_{A1} K_{A2} K_{A3} [NCS\text{-}1]^3) \quad (5)$$

where K_{A1}, K_{A2}, A_m, and A_d are defined as described above, K_{A3} is the association constant for adding a third NCS-1 monomer to the complex, and A_{tri} is the anisotropy of this species.

For each model, the values of the anisotropy of D2R-FL-containing species and their association constant(s) were estimated by nonlinear least-squares analysis with Origin 8 (OriginLab, Northampton, MA) or using MATLAB (Mathworks Inc., Natick, MA) routines developed in house. For these analyses, the total concentration of NCS-1 used in eqs 1−5 was used as an estimate of its free concentration, because [D2R-FL] $\ll K_{D,app}$, the apparent dissociation constant for the reaction, and the effect of ligand depletion can be ignored. The values and associated errors for the fitted parameters reflect the means and standard deviations obtained from at least three independent experiments, unless noted otherwise. The reported value for the reduced χ^2 is defined in ref 22.

The binding constant for an unlabeled D2R peptide (uD2R) was determined in a competition experiment in which D2R-FL was titrated with NCS-1 at fixed concentrations of the unlabeled peptide. The calculated anisotropy of the D2R-FL peptide in the presence of fixed concentrations of uD2R and varying concentrations of NCS-1 is given by eq 6 (competition model):

$$A_{calc} = (A_f + A_m K_{A1}[NCS\text{-}1]_f + A_d K_{A1} K_{A2} [NCS\text{-}1]_f^2) / (1 + K_{A1}[NCS\text{-}1]_f + K_{A1} K_{A2}[NCS\text{-}1]_f^2) \quad (6)$$

where the free concentration of NCS-1 and those of D2R-FL and uD2R are the simultaneous roots of mass balance equations for each species:

$$[NCS\text{-}1]_T = [NCS\text{-}1]_f (1 + K_{A1}[D2R\text{-}FL]_f + K'_{A1}[uD2R]_f) + [NCS\text{-}1]_f^2 (K_{A1} K_{A2}[D2R\text{-}FL]_f + K'_{A1} K'_{A2} [uD2R]_f) \quad (7a)$$

$$[D2R\text{-}FL]_T = [D2R\text{-}FL]_f + K_{A1}[NCS\text{-}1]_f [D2R\text{-}FL]_f + K_{A1} K_{A2}[NCS\text{-}1]_f^2 [D2R\text{-}FL]_f \quad (7b)$$

$$[uDR2]_T = [uD2R]_f + K'_{A1}[NCS\text{-}1]_f [uD2R]_f + K'_{A1} K'_{A2}[NCS\text{-}1]_f^2 [D2R\text{-}FL]_f \quad (7c)$$

In these experiments, the values of K_{A1}, K_{A2}, A_f, A_m, and A_d, determined in equivalent titrations in the absence of the unlabeled peptide, were used. The values of the association constants, K'_{A1} and K'_{A2}, for the unlabeled peptide were estimated from eqs 3b and 7a−c by minimizing the reduced χ^2 value between the experimental and calculated anisotropy values using MATLAB routines developed in house.

Analysis of titration curves for the effects of calcium ion concentration on the binding of the D2R-FL peptide to NCS-1 is described elsewhere (Supporting Information).

DNA Transfection and Co-Immunoprecipitation. HEK-293 cells were cultured in Dulbecco's modified Eagle's medium supplemented with 10% fetal bovine serum as previously described[4] and transfected with NCS-1 constructs containing either a C-terminal mycHis epitope tag (NCS-1-mycHis and NCS-1 ΔEF-mycHis) or a C-terminal hemagglutinin (HA) epitope tag (NCS-1-HA). Transient transfections were performed using the Effectine transfection reagent (Qiagen) under conditions described by the manufacturer.

Co-immunoprecipitations (coIPs) were conducted with lysates prepared from HEK-293 cells expressing various NCS-1 constructs. Lysates contained 100 μM $CaCl_2$ and 10 mM DTT. NCS-1-HA was immunoprecipitated with a rabbit anti-HA antibody (Covance). Western blot analysis of immunoprecipitated proteins was performed using a chicken anti-frequenin (anti-NCS-1) polyclonal antibody (1:14000 dilution, Rockland Immunochemicals). Immunoreactivity was detected with a horseradish peroxidase-conjugated secondary antibody (1:14000 dilution, Jackson Immuno-Research) and visualized using enhanced chemiluminescence (ECL plus, GE Healthcare).

Size Exclusion Chromatography Multiangle Laser Light Scattering (SEC-MALS). Analytical SEC-MALS measurements were taken using an Agilent 1200 series HPLC system (Agilent Technologies) equipped with an isocratic pump and autosampler. Chromatographic separations were accomplished using either a Superdex 75 10/300 GL or a 200 10/300 size exclusion column (GE Healthcare). The equilibration buffer and flow rate are given in the figure legends. Online measurements of statically scattered light were determined using a Wyatt Technologies DAWN HELEOS MALS detector with the concurrent change in the refractive index measured with a Wyatt Technologies Optilab rEX instrument. The assumed dn/dc (change in refractive index with concentration) value for these experiments was 0.185 mL/g. Data analysis, including molecular weight determination and sample polydispersity, was performed using the ASTRA V software package (Wyatt Technology). To minimize the MALS contribution of dust particles, solutions were prefiltered and in-line filtered with an Anodisc 0.1 μm filter membrane (Whatman).

Microbatch Multiangle Laser Light Scattering (MB-MALS). NCS-1 constructs were dialyzed into a buffer composed of 150 mM NaCl, 25 mM HEPES, 1 mM TCEP, and either 2 mM $CaCl_2$ or 1 mM EGTA (pH 7.5) and then filtered through an Anotop 0.02 μm syringe filter (Whatman). Samples at a known concentration were introduced into the flow cell of the Wyatt Technologies DAWN HELEOS detector using a syringe pump (Razel Scientific) at a constant flow rate of 0.15 mL/min. Samples were in-line filtered with an Anotop 0.02 μm syringe filter (Whatman). Light scattering data analysis and molecular weight measurements were conducted as described above after subtraction of a buffer baseline established at the beginning and end of each experiment.

Plots of molecular weight versus concentration and equilibrium dissociation constants for self-association were determined using Origin (OriginLab) curve fitting software. The monomer−dimer self-association model was fit to the observed molecular weight using the following relationship:

$$MW_{obs} = MW_{mon}\frac{C_{mon}}{C_{tot}} + 2MW_{mon}\frac{C_{dim}}{C_{tot}} \quad (8)$$

where MW_{obs} is the observed molecular weight, MW_{mon} is the molecular weight of the monomer, C_{mon} is the concentration of the monomer species, C_{dim} is the concentration of the dimer species, and C_{tot} is the total protein concentration. For any given total protein concentration expressed as a function of monomer (M_t) concentration, the concentration of the dimer species dependent on the equilibrium dissociation constant (K_d) can be given as

$$C_{dimer} = \left\{4M_t + K_d - \sqrt{-[(4M_t + K_d)^2 + 16M_t{}^2]}\right\}/8 \quad (9)$$

Values for K_d adjusted by nonlinear least-squares analysis were then used to determine dimer concentrations in eq 8.

Analytical Equilibrium Ultracentrifugation. Sedimentation equilibrium experiments were performed using a Beckman XL-A ultracentrifuge. NCS-1 samples were dialyzed into a buffer composed of 100 mM NaCl, 25 mM HEPES, 2 mM DTT, and 2 mM $CaCl_2$ or 1 mM EGTA (pH 7.5). Centrifugation experiments with initial protein concentrations between 0.1 and 0.8 mg/mL were performed at speeds ranging from 15000 to 30000 rpm at 20 °C using an An-60 Ti rotor. UV absorbance scans (278 nm) were collected in radial step mode with 0.001 cm steps averaged over five replicates. The models used for curve fitting the experimental data included a model corresponding to an ideal monomer and a self-associating ideal monomer−dimer system, which have been derived and discussed extensively elsewhere.[23,24] During data analysis, the solvent density was assumed to be 1.0, and the partial specific volume of NCS-1 was taken to be 0.730 cm^3/g, which was estimated from its amino acid sequence.[25]

Ligand Docking. The HADDOCK webserver[26] was used for flexible docking simulations of the peptide in the receptor binding site of NCS-1. The coordinates from chain A of Protein Data Bank (PDB) entry 1G8I were used as the rigid docking model for NCS-1. For the flexible receptor, residues 385−400 of PDB entry 3PBL were extracted and visualized in Chimera, and serine 399 was changed to histidine in its most commonly observed rotomer to match the sequence of the D2 peptide used in our assays. The structures of other NCS family members in complex with peptides were superimposed onto the structure of NCS-1. The peptides bound to similar parts of their respective proteins. The D2R peptide was superimposed onto the peptide helix of PDB entry 2I94. This placed residues D37 and L89 of the NCS-1 protein close to R391 and I397 of the D2R peptide. Therefore, these residues were set as active and the surrounding residues defined as passive in the analysis.

RESULTS AND DISCUSSION

Fluorescence Anisotropy Binding Isotherm for NCS-1 TEV. To determine whether the isolated D2R peptide (residues 428−443) binds NCS-1 TEV, a fluorescein-labeled version of this peptide, D2R-FL, was synthesized. Titration of 1 nM D2R-FL, in the presence of 2 mM $CaCl_2$, with increasing concentrations of nonmyristoylated NCS-1 TEV resulted in increases in the anisotropy of fluorescence polarization from ~0.04, for the free peptide, to a maximum value of ~0.23, at high NCS-1 concentrations (Figure 1). By contrast, in the absence of $CaCl_2$, no significant change in anisotropy was observed at 1 μM NCS-1 TEV and the increase was only 0.01 unit at 10 μM NCS-1 TEV (data not shown). The changes in anisotropy were not the result of alterations in the environment of the fluorophore in the presence of NCS-1, because the fluorescence intensity was unaffected throughout the titration[27] (see Figure SF1 of the Supporting Information). These data are consistent with D2R-FL binding to NCS-1 TEV in a specific and calcium-dependent manner.

The limiting anisotropy of the D2R-FL·NCS-1 TEV complex observed in the titration experiment is larger than expected for a 1:1 complex of an ~4 kDa peptide and a 22 kDa NCS-1 monomer and is more consistent with a 1:2 D2R-FL·NCS-1 complex. Therefore, to determine the stoichiometry and affinity of NCS-1 binding, the FA titration data were fit to each of five models: D2R-FL binds either one (model 1), two (model 2), or three (model 3) NCS-1 TEV monomers with perfect cooperativity (i.e., no significant intermediate species are present) or sequential assembly of two (model 4) or three (model 5) NCS-1 TEV monomers. Comparison of the χ^2 values for the fits of each model to the data indicates that only sequential binding model 4 accurately describes the data [χ^2 = 0.7 compared with χ^2 > 1.5 for models 1−3 and 5 (for a summary, see Table 1 and Figure SF2 of the Supporting Information)]. Moreover, a model in which D2R-FL and NCS-

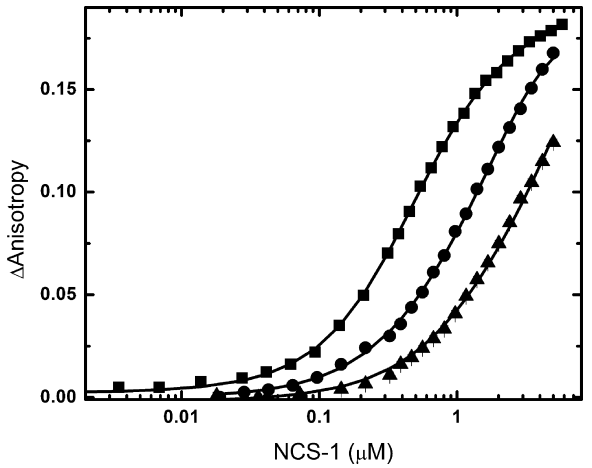

Figure 1. FA Titration of NCS-1 TEV. Anisotropy of 1 nM D2R-FL (■) is plotted as a function of increasing NCS-1 concentration at a fixed Ca^{2+} concentration. The error bars are small enough to be completely covered by the individual sample points. The solid black line shows the NLLS fit of model 4 to the data. This experiment was performed in triplicate. The D2F-FL peptide was also titrated with NCS-1 in the presence of 1 μM uD2R (●) or 5 μM (▲). The results of the fit of these data to the competition model are shown as the green solid line for the titration in the presence of 1 μM uD2R or as the red solid line in 5 μM uD2R.

1 form 2:2 complexes had a χ^2 value of >100 indicating that the complex contains only a single D2R-FL at these peptide concentrations (data not shown). In model 4, the D2R-FL peptide binds two monomers sequentially with dissociation constants for the first and second monomers of 0.27 ± 0.03 μM (K_{D1}) and 0.53 ± 0.06 μM (K_{D2}), respectively. Under these conditions, NCS-1 with and without 2 mM $CaCl_2$ was monomeric as determined by SEC-MALS [20.2 ± 0.3 and 22.1 ± 0.1 kDa, respectively (Figure SF3 of the Supporting Information)]. In addition, the concentration-normalized scattering curves of EGTA-treated (3 mg/mL) and calcium-loaded (6 mg/mL) NCS-1 were essentially identical as determined by small-angle X-ray scattering. Their radii of gyration (20.4 Å for EGTA and 20.8 Å for the calcium-loaded form) and longest vectors (60 Å for either) were also similar, indicating that they had the same shape in solution (Figure SF4 of the Supporting Information). In addition, the intensities extrapolated to zero angle and normalized for protein concentration [$I(0)/c$] are essentially the same, and the molecular masses calculated from the scattering intensity by the Porod method[28] were each 22 ± 10 kDa, in agreement with the calculated molecular mass of a monomer. Together, this suggests that the nonmyristoylated NCS-1 dimer formation observed in the FA binding experiments involves an allosteric transition resulting from D2R-FL peptide binding.

To determine the affinity of NCS-1 TEV for the unlabeled peptide, we performed a competition assay in which 1 nM D2R-FL was titrated in the presence of 0, 1, and 5 μM uD2R with increasing NCS-1 TEV concentrations (Figure 1). As expected, inclusion of the unlabeled peptide shifted the titration curves to higher NCS-1 TEV concentrations, with higher concentrations of uD2R having a stronger effect, indicating that the unlabeled peptide competes with D2R-FL for NCS-1 binding. Fitting of this data to the competition model, in which uD2R sequentially binds two NCS-1 monomers, accurately described the data ($\chi^2 \sim 1$ for all three uD2R peptide concentrations compared with values of >5 if the unlabeled peptide forms only 1:1 or 1:2 complexes with NCS-1). Under these conditions, the unlabeled peptide has an ~1.50-fold lower affinity (K'_{D1} = 0.39 ± 0.08 μM, and K'_{D2} = 0.81 ± 0.09 μM) for NCS-1 than for D2R-FL. The weaker affinity may reflect the effects of the carboxyl-terminal lysine residue and the fluorescein moiety in the D2R-FL peptide and/or aggregation of the unlabeled peptide at the concentrations used in these experiments. This latter possibility is supported by the observation that, in the presence of 10 μM uD2R, the measured anisotropy of the D2R-FL peptide alone was significantly higher [0.06 (data not shown)] than in its absence. The limited solubility of the D2R peptide used in this study precluded detailed structural analysis. In any case, the uD2R peptide binds NCS-1 with the same stoichiometry as and an affinity similar to that of D2R-FL, under our measurement conditions.

NCS-1 Can Oligomerize in Cell Lysates. The FA experiments imply that purified monomeric nonmyristoylated NCS-1 TEV can dimerize in the presence of the D2R-derived peptides. To assess whether NCS-1 can associate in cell lysates, we tested whether an anti-HA epitope-tagged antibody co-immunoprecipitated NCS-1-HA from lysates of HEK-293 cells expressing either NCS-1-HA alone or NCS-1-HA cotransfected with either NCS-1-mycHis or NCS-1 ΔEF-mycHis. The resultant blot was probed with an anti-NCS-1 antibody to detect the presence of either the HA-tagged or mycHis-tagged NCS-1 in the coIP (Figure 2). In untransfected cells, the anti-

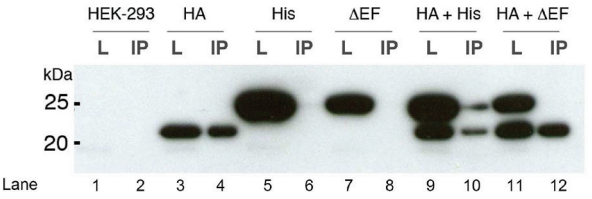

Figure 2. CoIP of the NCS-1·NCS-1 dimers. An anti-HA antibody was used to immunoprecipitate HA-tagged NCS-1 from crude membrane fractions of HEK-293 cells containing either no NCS-1-HA (HEK-293, lanes 1 and 2), NCS-1-HA (HA, lanes 3 and 4), NCS-1-mycHis (His, lanes 5 and 6), NCS-1 ΔEF-mycHis (ΔEF, lanes 7 and 8), NCS-1-HA and NCS-1-mycHis (HA + His, lanes 9 and 10), or NCS-1-HA and NCS-1 ΔEF-mycHis (HA + ΔEF, lanes 11 and 12). CoIPs were performed in the presence of 100 μM $CaCl_2$ and 10 mM DTT. The blot was probed using an anti-NCS-1 antibody. L indicates samples with lysate only, and IP indicates samples immunoprecipitated with the anti-HA antibody.

NCS-1 antibody failed to immunoreact with any cellular proteins (Figure 2, lanes 1 and 2). An immunoreactive band of ~22 kDa, the predicted size of HA-tagged NCS-1, was detected in lysates prepared from cells transfected with NCS-1 HA alone (Figure 2, lane 3). A band migrating with a similar molecular mass was detected in the immunoprecipitated (IP) lane (Figure 2, lane 4), indicating that the anti-HA antibody specifically immunoprecipitated NCS-1-HA from transfected cells. An immunoreactive band of ~25 kDa, the predicted size of NCS-1-mycHis, was detected in lysates prepared from cells transfected with NCS-1-mycHis alone (Figure 2, lane 5). However, no band was detected in the IP lane (Figure 2, lane 6), indicating that the NCS-1-mycHis protein did not immunoprecipitate with the anti-HA antibody. Similarly, an immunoreactive band of ~25 kDa was detected in lysates prepared from cells

transfected with the mycHis-tagged NCS-1 ΔEF variant (Figure 2, lane 7), whereas no band was detected in the NCS-1 ΔEF-mycHis IP lane (Figure 2, lane 8). Two bands, at ~22 and ~25 kDa, were detected in lysates from cells cotransfected with NCS-1-HA and NCS-1-mycHis (Figure 2, lane 9). Two bands with similar molecular masses were also detected in the IP lane (Figure 2, lane 10), indicating that NCS-1-HA and NCS-1-mycHis were coIP'd with anti-HA antibodies. Likewise, two bands at ~22 and ~25 kDa were detected in lysates prepared from cells cotransfected with NCS-1-HA and mycHis-tagged NCS-1 ΔEF (Figure 2, lane 11). However, only the 22 kDa NCS-1-HA protein was detected in the IP lane (Figure 2, lane 12). Therefore, the ~25 kDa mycHis-tagged NCS-1 ΔEF protein was unable to coIP with NCS-1-HA. Taken together, these coIP experiments indicate that NCS-1 can form oligomers in cell lysates. It is important to note that the ability of NCS-1 to form oligomers was dependent on the addition of calcium (100 μM $CaCl_2$) to the lysates, suggesting that NCS-1 oligomerization is mediated by physiologically relevant concentrations of localized calcium.[29,30] Our observation that the NCS-1 ΔEF-mycHis variant did not interact with NCS-1-HA, even in the presence of 100 μM calcium, further suggests that NCS-1 oligomerization is a calcium-dependent process, because this construct does not bind calcium but maintains proper secondary structure.[19] We therefore conclude that NCS-1 oligomerization was dependent on Ca^{2+} binding and requires functionally intact EF-hand domains, although we cannot determine whether oligomerization requires the presence of additional binding partners present in the lysate or is the result of myristoylation of NCS-1 in HEK-293 cells.

Myristoylated NCS-1 Can Form a Stable Calcium-Dependent Homodimer. To determine whether amino-terminal myristoylation affects NCS-1 oligomerization, we expressed and purified myristoylated NCS-1 with a carboxyl-terminal His_6 tag (MyrNCS-1 His_6).[19] Chromatography on a Superdex 75 column and in-line MALS analysis of EGTA-treated MyrNCS-1 His_6 revealed a single peak with the monomer molecular mass [21.5 ± 0.3 kDa (Figure 3A)]. By contrast, replacement of EGTA with 2 mM $CaCl_2$ in the sample and elution buffer resulted in the appearance of an additional peak corresponding to that of a stable dimeric species [46.7 ± 0.1 kDa (Figure 3B)], as well as a small amount of higher-molecular mass species. The higher-molecular mass species were not observed with nonmyristoylated NCS-1 His_6 under any condition tested (data not shown). In the presence of $CaCl_2$, the peak corresponding to the MyrNCS-1 His_6 monomer was broader and the leading edge had a molecular mass slightly larger than that of the monomer (~2−4 kDa). This leading edge effect was also observed in the absence of Ca^{2+} (Figure 3A). This lead us to conclude that dimerization of MyrNCS-1 His_6 involves two homodimeric species, one in rapid equilibrium (leading edge of main peak) that was weakly dependent on Ca^{2+} and the other, a stable homodimer (dimeric peak) that required Ca^{2+} bound to each of the three functional EF-hand domains. MyrNCS-1 His_6 dimerization was further characterized by MB-MALS (Figure SF5 of the Supporting Information) and analytical ultracentrifugation (Figure SF6 of the Supporting Information). In both cases, MyrNCS-1 His_6 formed a reversible dimer in the presence of 2 mM $CaCl_2$, but not in its absence. The dissociation constant for dimerization was found to be in the low micromolar range (10 ± 1 and 2 ± 0.2 μM by MB-MALS and analytical ultracentrifugation, respectively). These results confirm that myristoylated NCS-1

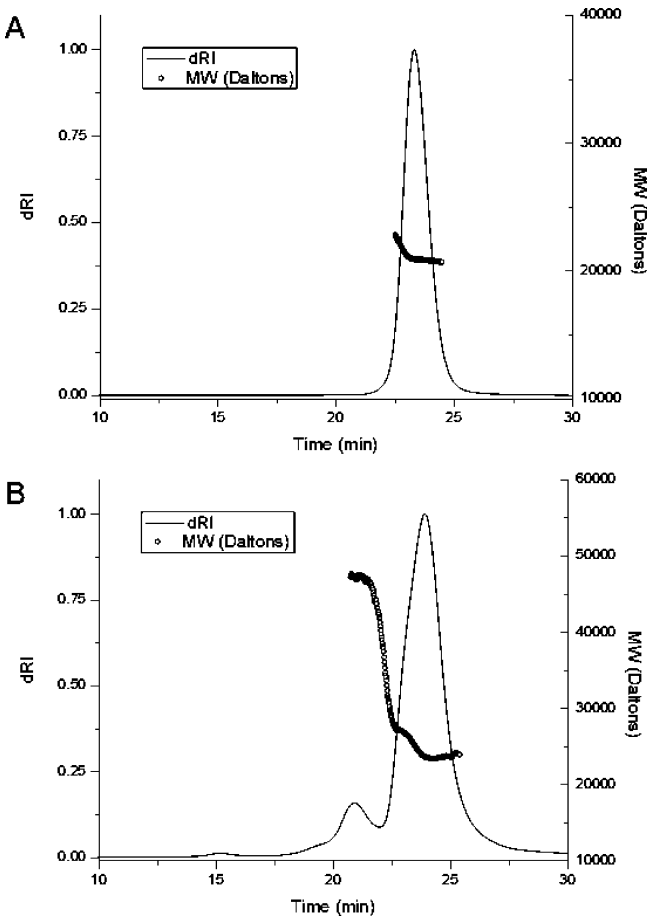

Figure 3. SEC-MALS analysis of the NCS-1 oligomeric state. Profiles of myristoylated 4 mg/mL NCS-1 His_6 in the (A) absence and (B) presence of calcium. The changes in the relative refractive index [right *y*-axis (—)] and molecular mass [left *y*-axis (○)] are given as a function of run time. The elution buffer for these experiments consisted of 25 mM Hepes (pH 7.5), 150 mM NaCl, 1 mM TCEP, and either 1 mM EGTA or 2 mM $CaCl_2$. Separations were conducted at a flow rate of 0.5 mL/min.

can form a calcium-dependent, reversible dimer in solution, which likely accounts for the dimerization observed in pull-down experiments from HEK-293 lysates. The Ca^{2+}- and myristoylation-dependent dimerization of NCS-1 observed here is similar to that reported for NCS family member VILIP-1.[31] MryNCS-1 His_6 was also capable of binding to the D2R-FL peptide, albeit with reduced affinity. Nonmyristoylated NCS-1 His_6 bound the D2R-FL peptide with an affinity similar to that of the NCS-1 TEV protein (for NCS-1 His_6, K_{D1} = 0.48 μM and K_{D2} = 1.3 μM, and for TEV protein, K_{D1} = 0.27 μM and K_{D2} = 0.53 μM). The slight decrease in the affinity of NCS-1 His_6 may reflect the effects of the tag on local ion concentrations around the protein. The MyrNCS-1 His_6 bound the D2R-FL peptide with an affinity lower than that of NCS-1 His_6 for both monomeric and dimeric complexes [K_{D1} = 3.4 ± 0.2, and K_{D2} = 5.9 ± 0.7 μM (Table 1 and Figure SF6 of the Supporting Information)]. The reduced affinity of the MyrNCS-1 His_6 construct could reflect competition between the myristoyl moiety, which is thought to bind to EF1, and the peptide for the same binding site in our solution-based assay or could be a result of a conformational change that reduces affinity.

dx.doi.org/10.1021/bi200637e | *Biochemistry* 2011, 50, 8780–8791

Table 1. Binding Isotherms of All NCS-1 Proteins[a]

construct	K_{D1} (μM)	K_{D2} (μM)	A_f	A_m	A_d	χ^2
NCS-1 TEV	0.27 ± 0.08	0.53 ± 0.09	0.045 ± 0.002	0.098 ± 0.007	0.236 ± 0.001	0.7
NCS-1 His_6	0.48 ± 0.05	1.3 ± 0.1	0.042 ± 0.007	0.092 ± 0.009	0.234 ± 0.003	0.8
E84Q	9 ± 1	71 ± 5	0.047 ± 0.003	0.10 ± 0.01	0.28 ± 0.05	1.3
E120Q	1.0 ± 0.1	7 ± 1	0.046 ± 0.003	0.102 ± 0.007	0.232 ± 0.005	0.9
E168Q	0.64 ± 0.07	8 ± 1	0.051 ± 0.005	0.10 ± 0.01	0.222 ± 0.003	1.1
NCS-1 ΔEF	NB	NB	NB	NB	NB	–
MyrNCS-1	3.4 ± 0.2	5.9 ± 0.7	0.044 ± 0.002	0.096 ± 0.009	0.238 ± 0.005	0.7

[a]Abbreviations: K_{D1}, equilibrium dissociation constant for the D2R-FL−NCS-1 monomer interaction; K_{D2}, equilibrium dissociation constant for the D2R-FL−NCS-1 dimer interaction; A_f, anisotropy of the unbound free D2R-FL; A_m, anisotropy of NCS-1 monomer-bound D2R-FL; A_d, anisotropy of dimer-bound D2R-FL; χ^2, χ^2 value of the fluorescence anisotropy curve fit; NB, no measurable binding.

Disruption of EF-Hands 2−4 Affects D2R Peptide Binding. Our previous work suggested a role for EF-hand 1 in binding to the D2R receptor.[4] Here, we demonstrate that binding of the isolated, fluorescently labeled D2R peptide (residues 428−443 of D2R) to NCS-1 also is calcium-dependent, and therefore, EF-hands 2−4 must play a role in peptide binding. To define the relative contributions of these EF-hands, we constructed and characterized, using a FA assay, variants of NCS-1 that prevented Ca^{2+} binding at specific sites (E84Q disrupts EF2, E120Q disrupts EF3, E168Q disrupts EF4, and ΔEF contains three point mutations to disrupt all functional EF-hands). These were chosen because they disrupt Ca^{2+} binding without significantly affecting NCS-1 structure.[19,32,33]

All of the single-site variants of NCS-1 were assayed in the NCS-1 His_6 background, because this construct was expressed at higher levels, which was beneficial for some of the poorly expressing variants. To account for the potential of altered binding affinities for D2R-FL caused by the affinity tag, NCS-1 His_6 was used for comparison. Titration of the three singly substituted nonmyristoylated NCS-1 His_6 variants revealed that each bound the D2R-FL, albeit with differing affinities. By contrast, the NCS-1 ΔEF construct, which disrupts all three calcium binding sites, displayed no observable binding even at 10 μM. Table 1 summarizes the parameters obtained (K_{D1}, K_{D2}, A_f, A_m, A_d, and reduced χ^2) for FA titrations of each variant fitted to model 4. The reported reduced χ^2 values with this model are all near unity, demonstrating the quality of the fits. None of the other binding models tested accurately described the titration curves, based upon the χ^2 criteria. Moreover, with model 4, there is good agreement between the fitted anisotropy values for each peptide-bound species for all of the NCS-1 variants, with the exception of A_d for NCS-1 E84Q, which is likely due to the presence of light scattering. Further, the limited solubility of this latter protein resulted in titration curves that reached only the K_d value, further reducing the quality of the fit. Taken together, these data support a binding model in which the isolated D2R peptide and NCS-1 form stable 1:1 and 1:2 complexes under the experimental conditions.

Analysis of the affinities of NCS-1 E84Q, E120Q, and E168Q for the D2R-FL peptide reveals that disruption of the Ca^{2+} binding site in EF2 (E84Q) results in the largest decrease in binding affinity for this peptide. The affinity of the first NCS-1 monomer is reduced by ∼15-fold and that of the second by >200-fold compared with that of NCS-1 His_6. The effect of the equivalent residue in EF3 (E120Q) was more modest (∼2- and 5-fold reductions in K_{D1} and K_{D2}, respectively), and disruption of Ca^{2+} binding by EF4 (E168Q) significantly affected only the value of K_{D2} (∼5-fold). These data suggest that all three Ca^{2+} binding sites contribute, in some manner, to the stability of D2R-FL·NCS-1 complexes.

Analysis of the values of the dissociation constants in light of the structure of NCS-1[34] provides insight into the possible individual roles of each EF-hand in D2R-FL binding. The NCS-1 E84Q mutation results in the largest increase in K_D values for both the monomer (K_{D1} ∼ 9 μM) and the dimer (K_{D2} ∼ 71 μM) when compared to the equivalent wild-type protein. The D2R interaction motif lies in the first 71 amino acids of NCS-1,[4] suggesting that EF2 affects the direct binding of NCS-1 to the D2R peptide. In addition, the significant destabilization of the 1:2 D2R-FL·NCS-1 complex suggests that Ca^{2+} binding at EF2 also contributes to the stability of NCS-1 dimer in the complex.

EF-hands within a protein typically occur in pairs that form discrete domains[35] allowing communication and positive cooperativity between them. Such coupling is seen in NCS-1 where EF1 and EF2 form a pair and EF3 and EF4 form a pair.[34] NCS-1 E120Q (EFΔ3) and NCS-1 E168Q (EFΔ4) both have minimal effects upon binding of the peptide to monomeric NCS-1 His_6 (K_{D1} values of 1.01 and 0.64 μM, respectively) compared to the K_{D1} of NCS-1 His_6 (0.48 μM). These minimal decreases may reflect either a slight alteration of the calcium binding affinity of EF2[32] or the fact that there are contributions to binding of the peptide from regions outside of EF1. Both substitutions (E120Q and E168Q) result in a modest decrease in the stability of the dimeric NCS-1 peptide complex (K_{D2} values of 7 and 8 μM, respectively) consistent with a supporting role in NCS-1 dimer formation in the complex. This similarity could be attributed to the structured pairing of these EF-hands, in that nonfunctionality of one affects the function of the other in dimer formation.

Effect of Calcium/Magnesium Ion Binding on the D2R-FL−NCS-1 Interaction. All three calcium ion binding EF-hands in NCS-1 contribute to D2R-FL peptide binding at saturating $CaCl_2$ concentrations. However, intracellular calcium concentrations are likely to be much lower than 2 mM. To investigate the calcium ion dependence of D2R peptide binding, we titrated 1 nM D2R-FL in the presence of 1 or 5 μM NCS-1 TEV with increasing concentrations of $CaCl_2$ (Figure 4). In the absence of calcium, a weak association between NCS-1 TEV and the D2R-FL peptide was observed as a small increase in anisotropy at high NCS-1 concentrations. This increase may be due to weak calcium ion-independent or nonspecific binding. Titration with $CaCl_2$ resulted in a biphasic increase in anisotropy that reached its maximum value at a Ca^{2+}:NCS-1 concentration ratio of ∼5:1. The limiting anisotropy value of each curve was dependent upon the

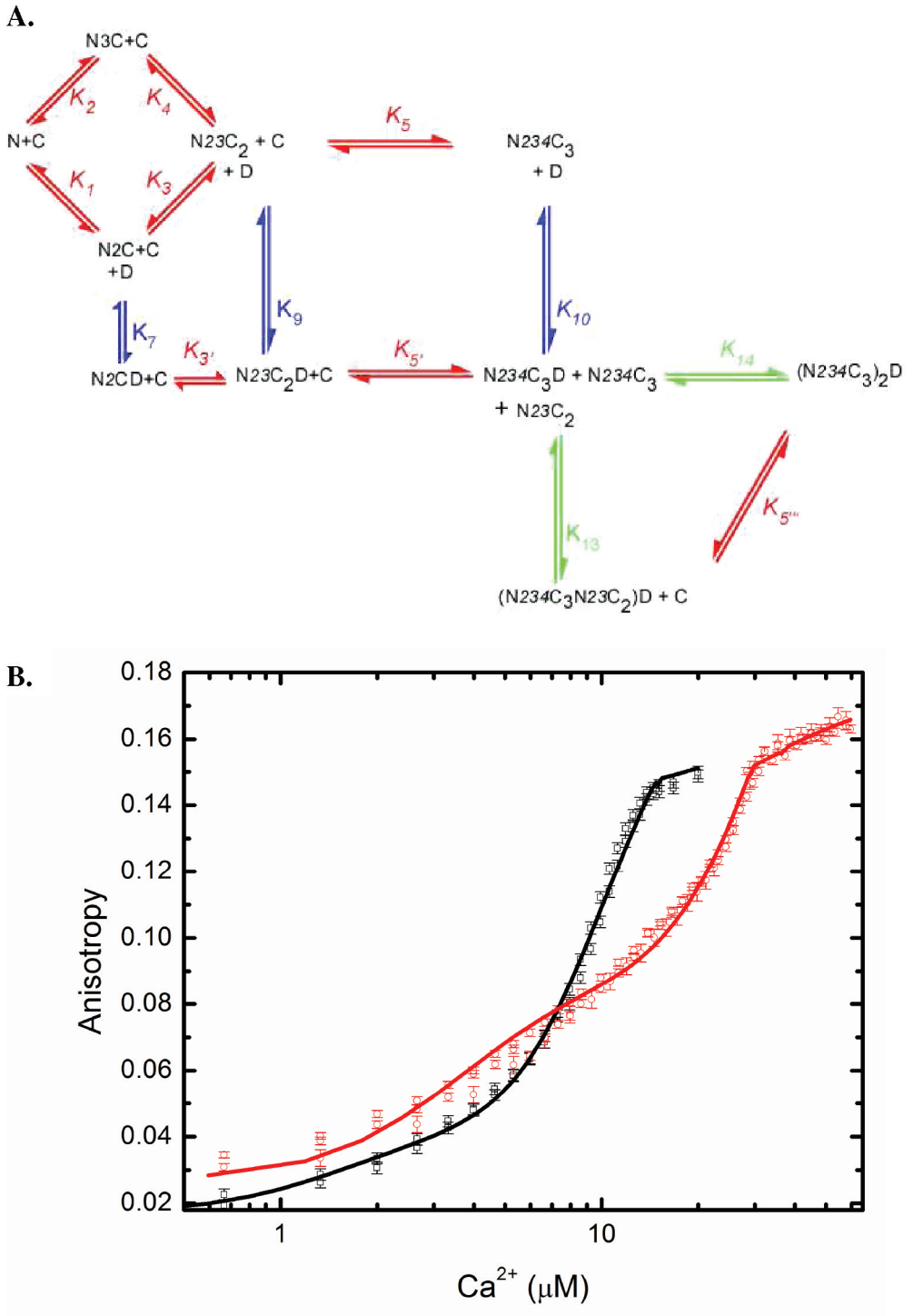

Figure 4. (A) FA calcium titration assay. (B) Anisotropy is plotted as a function of the total number of Ca^{2+} molecules per NCS-1 molecule. Sample titrations contained 1 nM D2R-FL and either 1 μM NCS-1 TEV (○) or 5 μM NCS-1 TEV (□). The solid lines represent the fitted anisotropy as described in the Supporting Information.

concentration of NCS-1 TEV in solution, suggesting that this concentration is limiting. This is in agreement with the peptide−NCS-1 titrations using 2 mM $CaCl_2$ described above. The biphasic nature of the anisotropy curve is consistent with the formation of both 1:1 and 1:2 D2R·NCS-1 complexes with differing dependencies on added Ca^{2+}.

A previous study has shown that nonmyristoylated NCS-1 binds Ca^{2+} independently in EF2−EF4.[36] In our studies, we observed a differential effect of Ca^{2+} binding at these sites upon binding of the D2R-FL peptide. To better characterize the Ca^{2+} dependence of complex formation, the $CaCl_2$ titration curves were fit to several binding models. Because of the complexity of the reaction, several assumptions were made. (1) In the absence of Ca^{2+}, NCS-1 binds nonspecifically to the D2R-FL peptide. (2) The anisotropies of the 1:1 and 1:2 D2R-FL·NCS-1 complexes are independent of the number of bound Ca^{2+} molecules. (3) Formation of the 1:2 D2R-FL·NCS-1 complex requires at least five total bound Ca^{2+} molecules. The first

dx.doi.org/10.1021/bi200637e | *Biochemistry* 2011, 50, 8780−8791

assumption appears valid because the dependence of the D2R-FL peptide anisotropy on NCS-1 concentration in the absence of $CaCl_2$ is low. Assumptions 2 and 3 were necessary to restrict the number of parameters to allow convergence of the fitting routines and thus represent clear limitations of the current model. Figure 4A is a schematic that describes the linkage between Ca^{2+} and D2R-FL binding to NCS-1. It fits the $CaCl_2$ titration data reasonably well [χ^2 values of 1.1 and 1.3 for the titrations with 1 and 5 μM NCS-1 TEV, respectively (see Supplemental Methods and Figure SF8 of the Supporting Information for details of this model)]. The key features of this model are as follows: (1) EF2 and EF3 bind randomly to Ca^{2+}, while the last site is filled only after the first two. (2) D2R-FL binds to only one of the mono Ca^{2+}-bound forms of NCS-1. (3) The 1:2 D2R-FL·NCS-1 dimer primarily contains six bound Ca^{2+} molecules. In this study, we propose that EF2 has the highest affinity for Ca^{2+} in the presence of the D2R-FL peptide and that occupancy of this site is sufficient to promote high-affinity binding of the peptide to the NCS-1 monomer. This is consistent with the significant reduction in binding affinity of the NCS-1 E84Q variant. The second sharp rise in the anisotropy, at an ~5:1 Ca^{2+}:NCS-1 ratio, likely corresponds to the formation of stable Ca^{2+}-saturated dimers bound to the D2R peptide. Because this occurs at higher concentrations of $CaCl_2$ and disruption of EF4 significantly affects only the 1:2 complexes (E168Q), we propose that binding of Ca^{2+} to EF4 accounts for the observed changes in anisotropy. A clear strength of this model is that it implies a role(s) for all three EF-hands in complex formation and is consistent with the NCS-1 TEV titration data obtained at saturating $CaCl_2$ concentrations. However, because of the simplifications necessary to obtain stable fits to the data and because Ca^{2+} binding is measured indirectly, the association constants for Ca^{2+} binding from these fits should be viewed with some caution.

Unlike other members of the NCS-1 family, two of the EF-hands (EF2 and EF3) can bind Mg^{2+} with micromolar affinity.[32] Because of the high cellular Mg^{2+} levels relative to those of Ca^{2+}, binding of magnesium ions could conceivably contribute to NCS-1 function.[32] To determine whether Mg^{2+} can substitute for Ca^{2+} in D2R peptide binding, we analyzed the effects of replacing Ca^{2+} with Mg^{2+}. In the absence of $CaCl_2$, all of the anisotropy values of the D2R-FL peptide in the presence of 5 μM NCS-1 TEV were identical and independent of $MgCl_2$ concentration (0−50 mM), demonstrating that NCS-1 TEV requires Ca^{2+} to interact with the D2R-FL. Because Mg^{2+} and Ca^{2+} share two binding sites on NCS-1, it is possible that the presence of Mg^{2+} could affect Ca^{2+}-dependent formation of the D2R-FL·NCS-1 complex. To test this idea, 1 nM D2R-FL and 5 μM NCS-1 TEV were titrated with $CaCl_2$ in the absence or presence of $MgCl_2$ concentrations ranging from 0 to 50 mM (Figure 5). Addition of 10 mM $MgCl_2$ (Figure 5A) altered the biphasic shape of the calcium FA titration curve compared to titrations without Mg^{2+}. At $MgCl_2$ concentrations of ≤10 mM, the measured anisotropy was elevated in the intermediate $CaCl_2$ range corresponding to Ca^{2+}:NCS-1 ratios from ~1:1 and 2.5:1. By contrast, at 50 mM $MgCl_2$, the measured anisotropy was lower than the corresponding values in its absence over the entire $CaCl_2$ concentration range measured (at 15 μM $CaCl_2$, the anisotropy decreases from 0.20 to 0.17 in the presence of 50 mM $MgCl_2$). This observation suggests that, at near physiological Mg^{2+} levels (<10 mM), Mg^{2+} can partially substitute for Ca^{2+} in stabilizing D2R·NCS-1 complexes;

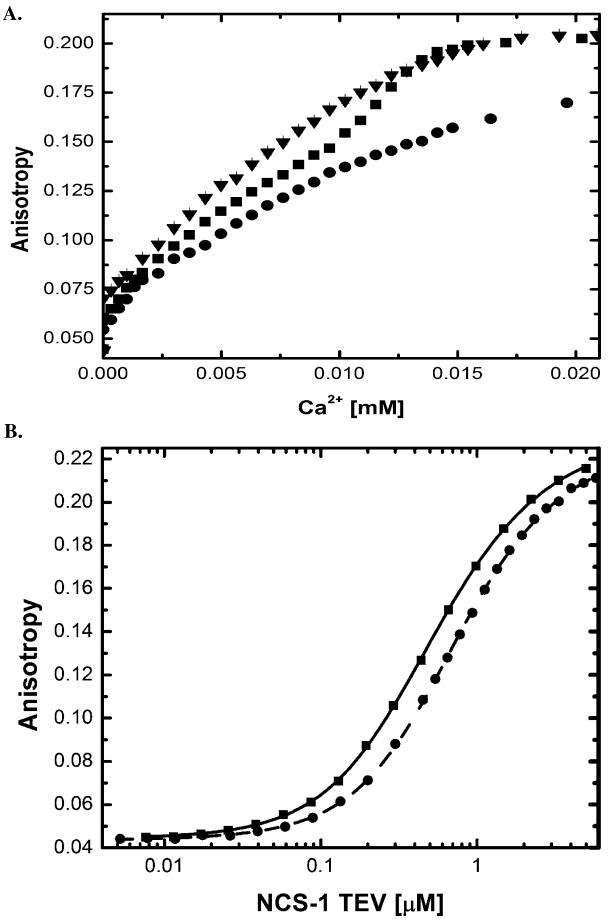

Figure 5. (A) Ca^{2+}/Mg^{2+} NCS-1 titrations. Anisotropy is plotted as a function of the total number of Ca^{2+} molecules per NCS-1 molecule. Error bars are small enough to be completely covered by individual sample points. Sample titrations contained 1 nM D2R-FL, 5 μM NCS-1 TEV, and either 0 (■), 10 (▼), or 50 mM Mg^{2+} (●). (B) Titration of 1 nM D2R-FL peptide with increasing NCS-1 concentrations, 5 mM $MgCl_2$, and 200 μM $CaCl_2$ (■; the solid line is the best fit to the data) or 200 μM $CaCl_2$ (●; the dashed line is the best fit to the data).

however, at higher levels, Mg^{2+} competes with Ca^{2+}. The enhanced stability of D2R-FL·NCS-1 complexes observed with 10 mM $MgCl_2$ may reflect occupancy of EF3 with Mg^{2+}, the relatively higher-affinity site for this ion (K_D ~ 17 μM). Because binding of Ca^{2+} by EF2 and EF3 appears to be sequential in the presence of the D2R-FL peptide and the affinity of EF2 for Mg^{2+} is much lower than that for Ca^{2+}, the presence of 10 mM $MgCl_2$ could allow occupancy of EF3 with Mg^{2+}, resulting in a higher proportion of NCS-1 TEV molecules having both EF2 and -3 occupied with divalent ions in the intermediate range of $CaCl_2$ concentrations. In this case, with EF2 occupied with Ca^{2+} and EF3 occupied with Mg^{2+}, NCS-1 TEV would be able to support binding of the D2R-FL peptide. The loss of binding observed at higher $MgCl_2$ concentrations could reflect binding of Mg^{2+} to EF2 preventing complex formation. This interpretation is consistent with the results of divalent ion binding studies with apo NCS-1[32] and the observation that the Ca^{2+} binding site in EF2 plays a critical in binding of D2R-FL.

Qualitatively, these results are consistent with a model in which Mg^{2+} can functionally replace Ca^{2+} at one of its low-affinity binding sites (EF3) but is a competitive inhibitor of binding to EF2. To further explore the possibility that physiological levels of Mg^{2+} and Ca^{2+} might play a role in

supporting formation of the D2R·NCS-1 complex, we titrated the D2R-FL peptide with NCS-1 TEV in the presence of 200 μM $CaCl_2$ with and without 5 mM $MgCl_2$ (Figure 5). In the presence of physiologically relevant Ca^{2+} and Mg^{2+} concentrations, the titration curve shifted to lower NCS-1 concentrations (K_{D1app} = 0.20 ± 0.04, K_{D2app} = 0.47 ± 0.02 μM, and χ^2 = 0.6; compared with K_{D1app} = 0.44 ± 0.05, K_{D2app} = 0.62 ± 0.02 μM, and χ^2 = 0.7 for the titration with $CaCl_2$ alone), suggesting that Mg^{2+} could act as a physiological cofactor with Ca^{2+} for binding.

Modeling of the D2R-FL Peptide Binding Site in NCS-1. To interpret the biochemical data in a structural context, we docked the peptide into the crystal structure of NCS-1 (PDB entry 1G8I). The crystal structure of the D3 receptor (D3R) was recently determined,[37] which also binds NCS-1.[4] It contains a sequence that is virtually identical to the D2R peptide used in our studies. In the context of the D3R structure, the D2R peptide appears to form an α-helix. To model the interaction between NCS-1 and the D2R peptide, the coordinates of this region in the D3 structure were extracted and the sequence was changed to agree with D2R by replacing the serine with the most commonly observed rotomer of histidine. Three structures of NCS family members in complexes with peptides are currently available (PDB entries 1S6C, 2I94, and 2JU0). Although the details of binding are different in each case, they share a common binding site for their substrates (PDB entry 1S6C, residues 217−225 of the potassium voltage-gated subfamily D member 2; PDB entry 2I94, residues 1−16 of rhodopsin kinase; PDB entry 2JU0, residues 145−169 of phosphatidylinositol 4-kinase) that binds to EF1 and helix 5 (within EF2). The D2R peptide was superimposed onto the bound peptide helix of PDB entry 2I94, and its new position was used as starting coordinates for docking of the D2R peptide onto the surface of NCS-1. The docking algorithm was run multiple times with different constraints. The models that gave the best composite scores bound the peptide in a similar orientation; a representative model is shown in Figure 6. To visualize the dimer, the coordinates of neurocalcin were used (PDB entry 1BJF)[38] as a template, and the coordinates of NCS-1 superimposed on each monomer. This allowed us to estimate the distance between the two D2R putative binding sites on NCS-1, which were approximately 45 Å apart. An interesting feature of this peptide binding site is the fact that it overlaps with the myristoyl-binding pocket identified in NCS homologue GCAP-1.[39] Like NCS-1,[40] the myristoyl moiety is not involved in a calcium-myristoyl switch and thus interacts with the protein in the Ca^{2+} free state. This would provide an explanation for the reduced affinity of Myr-NSC-1 for the D2R peptide, because it would have to compete with the myristoyl moiety for binding. However, in the presence of a membrane bilayer, the myristoyl moiety is likely to interact with the bilayer and not with NCS-1, relieving inhibition.

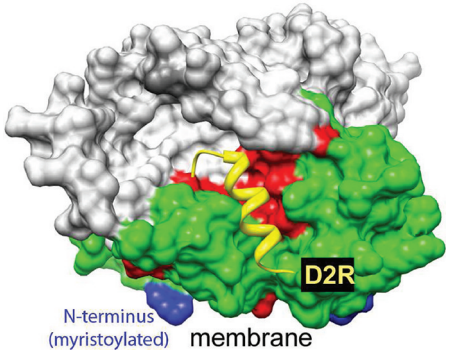

Figure 6. Model of the putative NCS-1 dimer with the D2R peptide. The molecular surface of the NCS-1 dimer is colored according to EF-hand: green for EF1 (residues 2−59), red for EF2 (residues 60−95), and gray for EF3 and EF4 (residues 96−190). The amino-terminal residue is colored blue. The D2R peptide is shown as a yellow helix. This figure was produced using Chimera.[45]

CONCLUSIONS

At physiological concentrations of Ca^{2+} and Mg^{2+}, the three functional EF-hands in NCS-1 support D2R peptide binding. Currently, there are no high-resolution structures for the complex between NCS-1 and the D2R or D3R receptor, and thus, the binding site on NCS-1 for the peptide cannot be identified unambiguously. However, deletion of EF1 (residues 1−60) abrogates D2R binding,[4] and disruption of Ca^{2+} binding in EF2, which pairs with EF1, severely affects D2R peptide binding. In contrast, disruption of Ca^{2+} binding in either EF3 or EF4 primarily affects dimerization. This suggests that the D2R peptide binds to the first 60 residues of NCS-1. In our structural model, the peptide binds within EF1 with its N-terminus on the same face as the membrane-anchored myristoylated N-terminus of NCS-1 (Figure 6), as is observed in other NCS family members.[38,41] This placement is consistent with the observed reduction in affinity for the D2R peptide for myristoylated NCS-1. In the absence of a membrane, the myristoyl moiety is thought to interact with EF1 and, thus, in our solution experiments would directly compete with the fluorescently labeled D2R peptide. The NCS-1 monomer has a hydrophobic groove that runs the length of the protein. Although we cannot rule out binding of the D2R peptide within this groove, it seems unlikely, as it would place the N-terminus of the D2R peptide farther from the plasma membrane.

To model the NCS-1 dimer, we used neurocalcin, a dimeric member of the NCS family. In neurocalcin, the hydrophobic groove is shorter, because of the different packing of the C-terminal helix.[38] The residues in the interface are largely conserved in NCS-1, raising the possibility that the receptor binding to EF1 in Ca^{2+}-loaded NCS-1 could trigger a conformational change in the C-terminal helix that promotes dimerization in a similar way. The enhanced dimerization of myristoylated NCS-1 may reflect a general effect of occupancy of EF1. This model would also explain why NCS-1 is monomeric in its complex with PI4Kβ,[42] because both the C-terminal helix and PI4Kβ utilize the same binding surface. In our model, the contributions of D2R peptide and divalent cation binding are similar to that of divalent cation binding to the myristoylated form of VILIP-1.[31] In any case, the question of why NCS-1 dimerizes at all remains. One possible explanation is that the NCS-1 dimer stabilizes its interaction with the D2 and D3 receptors, which are themselves dimeric.[43] In this highly speculative model, the two putative D2R peptide binding sites are ~45 Å apart. On the basis of the crystal structure of the D3R−lysozyme chimera, the two NCS-1 binding helices (named helix VII) sit approximately parallel to the plane of the membrane and perpendicular to the transmembrane helices. If each helix VII changed orientation upon NCS-1 binding to become perpendicular to the surface of the membrane, the two helix VII forms would be approximately

45 Å apart and a 2:2 D2R-FL·NCS-1 complex could form. Although we did not observe a 2:2 D2R-FL·NCS-1 complex, the biochemical experiments were performed at low peptide concentrations and high NCS-1 concentrations. These conditions favor 1:2 complexes. Alternatively, the 1:2 D2R·NCS-1 complex that we observed may allow recruitment of other factors to the signalsome modulating the activity of the receptor complex.[44] The answer to these critical questions will require a high-resolution structure of the D2R·NCS-1 complex. The results presented here do highlight the possibility of using FA as a high-throughput tool to screen for compounds capable of specifically blocking the association between the D2R and NCS-1.

■ ASSOCIATED CONTENT

Supporting Information

Methods, one table, eight figures and six supplemental references. This material is available free of charge via the Internet at http://pubs.acs.org.

■ AUTHOR INFORMATION

Corresponding Author

*Department of Biochemistry, Pennsylvania State University College of Medicine, Hershey, PA 17033. Telephone: (717) 531-4189. Fax: (717) 531-7072. E-mail: jmf27@psu.edu.

Author Contributions

M.W. and D.C. contributed equally to this work.

Funding

We acknowledge financial support from the National Institute on Drug Abuse (DA025995, R.L.) and a grant from the Pennsylvania Department of Health using Tobacco Settlement Funds.

■ ACKNOWLEDGMENTS

We thank Drs. Jorg Roesgen and Ira Ropson for a careful reading of the manuscript. Molecular graphics images were produced using the UCSF Chimera package from the Resource for Biocomputing, Visualization, and Informatics at the University of California, San Francisco (supported by National Institutes of Health Grant P41 RR001081). We thank Drs. Marc Allaire and Lin Yang from X9 at the National Synchrotron Light Source (Brookhaven National Laboratory, Upton, NY) for their support and discussions. Use of the National Synchrotron Light Source was supported by the U.S. Department of Energy, Office of Science, Office of Basic Energy Sciences, under Contract DE-AC02-98CH10886.

■ ABBREVIATIONS

Ca^{2+}, calcium; D2R, D2 dopamine receptor; NCS-1, neuronal calcium sensor-1; FA, fluorescence anisotropy; D2R-FL, fluorescein-labeled D2 dopamine receptor peptide; uD2R, unlabeled D2 dopamine receptor peptide.

■ REFERENCES

(1) Burgoyne, R. D., O'Callaghan, D. W., Hasdemir, B., Haynes, L. P., and Tepikin, A. V. (2004) Neuronal Ca^{2+}-sensor proteins: Multitalented regulators of neuronal function. *Trends Neurosci. 27*, 203−209.

(2) Nef, S., Fiumelli, H., de Castro, E., Raes, M. B., and Nef, P. (1995) Identification of neuronal calcium sensor (NCS-1) possibly involved in the regulation of receptor phosphorylation. *J. Recept. Signal Transduction Res. 15*, 365−378.

(3) McFerran, B. W., Graham, M. E., and Burgoyne, R. D. (1998) Neuronal Ca^{2+} sensor 1, the mammalian homologue of frequenin, is expressed in chromaffin and PC12 cells and regulates neurosecretion from dense-core granules. *J. Biol. Chem. 273*, 22768−22772.

(4) Kabbani, N., Negyessy, L., Lin, R., Goldman-Rakic, P., and Levenson, R. (2002) Interaction with neuronal calcium sensor NCS-1 mediates desensitization of the D2 dopamine receptor. *J. Neurosci. 22*, 8476−8486.

(5) Handley, M. T., Lian, L. Y., Haynes, L. P., and Burgoyne, R. D. (2011) Structural and functional deficits in a neuronal calcium sensor-1 mutant identified in a case of autistic spectrum disorder. *PLoS One 5*, e10534.

(6) Koh, P. O., Undie, A. S., Kabbani, N., Levenson, R., Goldman-Rakic, P. S., and Lidow, M. S. (2003) Up-regulation of neuronal calcium sensor-1 (NCS-1) in the prefrontal cortex of schizophrenic and bipolar patients. *Proc. Natl. Acad. Sci. U.S.A. 100*, 313−317.

(7) Lidow, M. S. (2003) Calcium signaling dysfunction in schizophrenia: A unifying approach. *Brain Res. Brain Res. Rev. 43*, 70−84.

(8) Nakamura, T. Y., Jeromin, A., Smith, G., Kurushima, H., Koga, H., Nakabeppu, Y., Wakabayashi, S., and Nabekura, J. (2006) Novel role of neuronal Ca^{2+} sensor-1 as a survival factor up-regulated in injured neurons. *J. Cell Biol. 172*, 1081−1091.

(9) Aronica, E., Boer, K., Doorn, K. J., Zurolo, E., Spliet, W. G., van Rijen, P. C., Baayen, J. C., Gorter, J. A., and Jeromin, A. (2009) Expression and localization of voltage dependent potassium channel Kv4.2 in epilepsy associated focal lesions. *Neurobiol. Dis. 36*, 81−95.

(10) Kawasaki, H., and Kretsinger, R. H. (1994) Calcium-binding proteins. 1: EF-hands. *Protein Profile 1*, 343−517.

(11) Burgoyne, R. D., and Weiss, J. L. (2001) The neuronal calcium sensor family of Ca^{2+}-binding proteins. *Biochem. J. 353*, 1−12.

(12) Rajebhosale, M., Greenwood, S., Vidugiriene, J., Jeromin, A., and Hilfiker, S. (2003) Phosphatidylinositol 4-OH kinase is a downstream target of neuronal calcium sensor-1 in enhancing exocytosis in neuroendocrine cells. *J. Biol. Chem. 278*, 6075−6084.

(13) Weiss, J. L., Archer, D. A., and Burgoyne, R. D. (2000) Neuronal Ca^{2+} sensor-1/frequenin functions in an autocrine pathway regulating Ca^{2+} channels in bovine adrenal chromaffin cells. *J. Biol. Chem. 275*, 40082−40087.

(14) Haynes, L. P., Fitzgerald, D. J., Wareing, B., O'Callaghan, D. W., Morgan, A., and Burgoyne, R. D. (2006) Analysis of the interacting partners of the neuronal calcium-binding proteins L-CaBP1, hippocalcin, NCS-1 and neurocalcin delta. *Proteomics 6*, 1822−1832.

(15) Cox, J. A., Durussel, I., Comte, M., Nef, S., Nef, P., Lenz, S. E., and Gundelfinger, E. D. (1994) Cation binding and conformational changes in VILIP and NCS-1, two neuron-specific calcium-binding proteins. *J. Biol. Chem. 269*, 32807−32813.

(16) Osawa, M., Dace, A., Tong, K. I., Valiveti, A., Ikura, M., and Ames, J. B. (2005) Mg^{2+} and Ca^{2+} differentially regulate DNA binding and dimerization of DREAM. *J. Biol. Chem. 280*, 18008−18014.

(17) Dizhoor, A. M., Olshevskaya, E. V., and Peshenko, I. V. (2010) Mg^{2+}/Ca^{2+} cation binding cycle of guanylyl cyclase activating proteins (GCAPs): Role in regulation of photoreceptor guanylyl cyclase. *Mol. Cell. Biochem. 334*, 117−124.

(18) Permyakov, S. E., Nazipova, A. A., Denesyuk, A. I., Bakunts, A. G., Zinchenko, D. V., Lipkin, V. M., Uversky, V. N., and Permyakov, E. A. (2007) Recoverin as a redox-sensitive protein. *J. Proteome Res. 6*, 1855−1863.

(19) De Cotiis, D. A., Woll, M. P., Fox, T. E., Hill, R. B., Levenson, R., and Flanagan, J. M. (2008) Optimized expression and purification of myristoylated human neuronal calcium sensor 1 in *E. coli*. *Protein Expression Purif. 61*, 103−112.

(20) Studier, F. W. (2005) Protein production by auto-induction in high density shaking cultures. *Protein Expression Purif. 41*, 207−234.

(21) Riddles, P. W., Blakeley, R. L., and Zerner, B. (1983) Reassessment of Ellman's reagent. *Methods Enzymol. 91*, 49−60.

(22) Bevington, P. R., and Robinson, D. K. (1992) *Data Reduction and Error Analysis for The Physical Sciences*, McGraw-Hill, New York.

(23) Lebowitz, J., Lewis, M. S., and Schuck, P. (2002) Modern analytical ultracentrifugation in protein science: A tutorial review. *Protein Sci. 11*, 2067−2079.
(24) Minton, A. P. (1990) Quantitative characterization of reversible molecular associations via analytical centrifugation. *Anal. Biochem. 190*, 1−6.
(25) Harpaz, Y., Gerstein, M., and Chothia, C. (1994) Volume changes on protein folding. *Structure 2*, 641−649.
(26) de Vries, S. J., van Dijk, M., and Bonvin, A. M. (2010) The HADDOCK web server for data-driven biomolecular docking. *Nat. Protoc. 5*, 883−897.
(27) Roehrl, M. H., Wang, J. Y., and Wagner, G. (2004) Discovery of small-molecule inhibitors of the NFAT−calcineurin interaction by competitive high-throughput fluorescence polarization screening. *Biochemistry 43*, 16067−16075.
(28) Feigin, L. A., and Svergun, D. I. (1987) *Structure Analysis by Small Angle X-ray and Neutron Scattering*, Plenum Press, New York.
(29) Ben-Jonathan, N., and Hnasko, R. (2001) Dopamine as a prolactin (PRL) inhibitor. *Endocr. Rev. 22*, 724−763.
(30) Langley, K., and Grant, N. J. (1997) Are exocytosis mechanisms neurotransmitter specific? *Neurochem. Int. 31*, 739−757.
(31) Li, C., Pan, W., Braunewell, K. H., and Ames, J. B. (2011) Structural analysis of Mg^{2+} and Ca^{2+} binding, myristoylation, and dimerization of the neuronal calcium sensor and visinin-like protein 1 (VILIP-1). *J. Biol. Chem. 286*, 6354−6366.
(32) Aravind, P., Chandra, K., Reddy, P. P., Jeromin, A., Chary, K. V., and Sharma, Y. (2008) Regulatory and structural EF-hand motifs of neuronal calcium sensor-1: Mg^{2+} modulates Ca^{2+} binding, Ca^{2+}-induced conformational changes, and equilibrium unfolding transitions. *J. Mol. Biol. 376*, 1100−1115.
(33) Muralidhar, D., Jobby, M. K., Krishnan, K., Annapurna, V., Chary, K. V., Jeromin, A., and Sharma, Y. (2005) Equilibrium unfolding of neuronal calcium sensor-1: N-terminal myristoylation influences unfolding and reduces protein stiffening in the presence of calcium. *J. Biol. Chem. 280*, 15569−15578.
(34) Bourne, Y., Dannenberg, J., Pollmann, V., Marchot, P., and Pongs, O. (2001) Immunocytochemical localization and crystal structure of human frequenin (neuronal calcium sensor 1). *J. Biol. Chem. 276*, 11949−11955.
(35) Gifford, J. L., Walsh, M. P., and Vogel, H. J. (2007) Structures and metal-ion-binding properties of the Ca^{2+}-binding helix-loop-helix EF-hand motifs. *Biochem. J. 405*, 199−221.
(36) Chandra, K., Ramakrishnan, V., Sharma, Y., and Chary, K. V. (2011) N-terminal myristoylation alters the calcium binding pathways in neuronal calcium sensor-1. *J. Biol. Inorg. Chem. 16*, 81−95.
(37) Chien, E. Y., Liu, W., Zhao, Q., Katritch, V., Han, G. W., Hanson, M. A., Shi, L., Newman, A. H., Javitch, J. A., Cherezov, V., and Stevens, R. C. (2010) Structure of the human dopamine D3 receptor in complex with a D2/D3 selective antagonist. *Science 330*, 1091−1095.
(38) Vijay-Kumar, S., and Kumar, V. D. (1999) Crystal structure of recombinant bovine neurocalcin. *Nat. Struct. Biol. 6*, 80−88.
(39) Stephen, R., Bereta, G., Golczak, M., Palczewski, K., and Sousa, M. C. (2007) Stabilizing function for myristoyl group revealed by the crystal structure of a neuronal calcium sensor, guanylate cyclase-activating protein 1. *Structure 15*, 1392−1402.
(40) Chandra, K., Sharma, Y., and Chary, K. V. (2011) Characterization of low-energy excited states in the native state ensemble of non-myristoylated and myristoylated neuronal calcium sensor-1. *Biochim. Biophys. Acta 1814*, 334−344.
(41) Lim, S., Strahl, T., Thorner, J., and Ames, J. B. (2011) Structure of a Ca^{2+}-myristoyl switch protein that controls activation of a phosphatidylinositol 4-kinase in fission yeast. *J. Biol. Chem. 286*, 12565−12577.
(42) Strahl, T., Huttner, I. G., Lusin, J. D., Osawa, M., King, D., Thorner, J., and Ames, J. B. (2007) Structural insights into activation of phosphatidylinositol 4-kinase (Pik1) by yeast frequenin (Frq1). *J. Biol. Chem. 282*, 30949−30959.
(43) Armstrong, D., and Strange, P. G. (2001) Dopamine D2 receptor dimer formation: Evidence from ligand binding. *J. Biol. Chem. 276*, 22621−22629.
(44) Kabbani, N., and Levenson, R. (2007) A proteomic approach to receptor signaling: Molecular mechanisms and therapeutic implications derived from discovery of the dopamine D2 receptor signalplex. *Eur. J. Pharmacol. 572*, 83−93.
(45) Pettersen, E. F., Goddard, T. D., Huang, C. C., Couch, G. S., Greenblatt, D. M., Meng, E. C., and Ferrin, T. E. (2004) UCSF Chimera: A visualization system for exploratory research and analysis. *J. Comput. Chem. 25*, 1605−1612.